

Multidome superconductivity in charge density wave kagome metals

Yu-Ping Lin¹ and Rahul M. Nandkishore^{1,2}

¹*Department of Physics, University of Colorado, Boulder, Colorado 80309, USA*

²*Center for Theory of Quantum Matter, University of Colorado, Boulder, Colorado 80309, USA*

(Dated: August 31, 2022)

Motivated by recent experiments on the kagome metals AV_3Sb_5 with $A = K, Rb,$ and Cs , which show a charge density wave (CDW) at ~ 100 K and the superconductivity at ~ 1 K, we explore the onset of the superconductivity, taking the perspective that it descends from a parent CDW. We argue that viewing the superconductivity as a weak-coupling instability of a reconstructed (by the CDW) Fermi surface naturally explains the experimentally observed ‘multidome’ nonmonotonic dependence on pressure, with the ‘peaks’ in the superconducting critical temperature being associated with the Van Hove singularities of the reconstructed Fermi surface. This ‘parent-child relationship’ also naturally explains the large separation of energy scales between the superconductivity and the CDW. We discuss different possible pairing mechanisms and speculate that the CDW or reconstructed Pomeranchuk fluctuations may mediate the pairing interaction.

Introduction.—The correlated phenomena in the recently uncovered kagome metals AV_3Sb_5 with $A = K, Rb,$ and Cs have drawn enormous attention. Charge density waves (CDWs) were observed at high critical temperature $T_{CDW} \sim 100$ K [1–29]. With simultaneous ordering at three commensurate momenta, these $3Q$ orders are believed to be driven by the Fermi surface nesting, further enhanced by the Van Hove singularity (VHS) [30]. The bond density modulations form (inverse) star-of-David patterns [31–39] with possible higher-order topology [40]. Meanwhile, the giant anomalous Hall effects indicate a band topology with time-reversal symmetry breaking [2, 7], which may be attributed to the loop currents [5, 17, 20, 26, 32–35, 37, 41–46]. On the other hand, the C_3 symmetry breaking is generally observed and is possibly induced by the three-dimensional orders [35, 38, 39].

More exotic observations appeared in the superconductivity (SC) [3, 6, 8, 10, 12, 22–24, 27, 29, 47–55]. The superconductivity develops at much lower critical temperature $T_{SC} \sim 1$ K with the C_3 symmetry breaking persisting [52, 53]. Remarkably, the superconductivity exhibits a double-dome structure under pressure, which extends above the critical pressure of the CDW [6, 8, 24, 27]. New superconducting domes can even appear at much higher pressure [8, 51, 55]. Despite the rich experimental observations, a thorough theoretical understanding remains elusive. Given the proximity to the VHS, the superconductivity may be treated as a competing instability with the CDW [56]. This scenario may explain the opposite trends of T_{CDW} and T_{SC} in certain experimental regimes, such as under pressure [6, 8, 24, 27, 51, 55] and uniaxial strain [29]. However, the scenario does not fit the large separation of energy scales between the superconductivity and the CDW, nor does it explain the double-dome superconductivity under the monotonically suppressed CDW. An alternative scenario is thus suggested for the origin of the superconductivity.

In this Research Letter, we propose an alternative sce-

nario that appears consistent with the salient experimental facts. We adopt the perspective that the CDW is a ‘parent’ phase, and that the ‘child’ superconductivity emerges from the reconstructed Fermi surface thereof. This ‘parent-child relationship’ not only naturally explains the large separation of energy scales between the superconductivity and the CDW but also predicts a multidome structure for the superconductivity (Fig. 1) [6, 24, 27], with the critical temperature enhanced near the (reconstructed) VHSs. We further discuss possible pairing mechanisms and speculate that the CDW or reconstructed Pomeranchuk (RPOM) fluctuations may mediate the pairing interaction.

CDW kagome metal.—Our analysis focuses on the Van Hove (VH) CDW on the middle band of the kagome lattice. At the VHS, the Fermi surface is a hexagon in

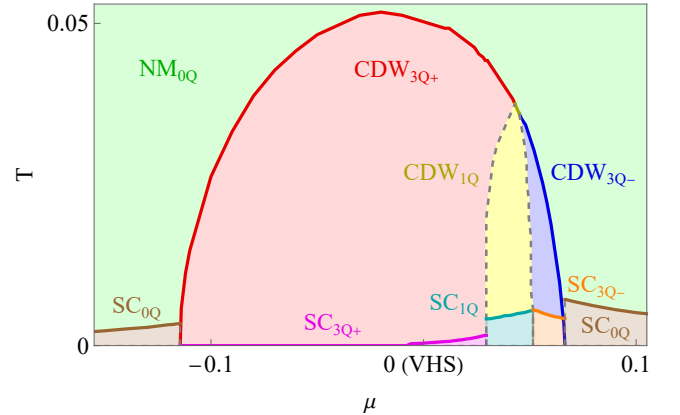


FIG. 1. Phase diagram of the parent CDW and the multidome child superconductivity. The CDW is computed from the free energy (1) with $\Lambda_k = 1$. The dispersion coefficients $A_+ = 3.15$ and $A_- = 1.45$ are set according to the tight-binding model for Figs. 2 and 3. The interaction $V_{CDW} = 25$ is chosen to approach the large gap in the experiment [19]. The critical temperature of the superconductivity T_{SC} [Eqs. (8) and (15)] is estimated with $\Lambda_{SC} = 0.01$ and $C_{SC} = 2$.

the hexagonal Brillouin zone (BZ). The corner saddle points sit at the zone edge centers $\mathbf{M}_{\alpha=1,2,3}$ [Figs. 2(a) and 2(b)], where the particle-type dispersion energy reads $\varepsilon_{\alpha\mathbf{k}} = A_+ k_{\alpha+}^2 - A_- k_{\alpha-}^2$ with $A_{\pm} > 0$ for small relative momenta ($k_{\alpha+}, k_{\alpha-}$) from \mathbf{M}_{α} . The density of states experiences the logarithmic VHS at these points [30], which enhances the Fermi liquid instabilities in various channels [35, 46, 57–64]. In particular, the Fermi surface nesting can enhance the CDW at three commensurate nesting momenta $\mathbf{Q}_{\alpha} \equiv \mathbf{M}_{\alpha}$. Due to the doubled periodicity $2\mathbf{Q}_{\alpha} \equiv 0$, the bands are folded quadruply onto the $1/2 \times 1/2$ reduced BZ. The CDW then opens the gaps and shrinks the reconstructed Fermi surface.

We choose the real CDW $\vec{\Delta} = (\Delta_1, \Delta_2, \Delta_3)$ specifically to exemplify our analysis. The energetically favored ground states can be determined by minimizing the mean-field free energy [65]

$$f[\vec{\Delta}] = \frac{2}{V_{\text{CDW}}} - \sum_n \int_{\mathbf{k}} \ln[1 + e^{-(E_{n\mathbf{k}}[\vec{\Delta}] - \mu)/T}]. \quad (1)$$

Each energy $E_{n\mathbf{k}}[\vec{\Delta}]$ is an eigenvalue of the effective Hamiltonian

$$H_{\text{CDW},\mathbf{k}}[\vec{\Delta}] = \begin{pmatrix} \varepsilon_{1\mathbf{k}} & -\Delta_3 & -\Delta_2 \\ -\Delta_3 & \varepsilon_{2\mathbf{k}} & -\Delta_1 \\ -\Delta_2 & -\Delta_1 & \varepsilon_{3\mathbf{k}} \end{pmatrix}, \quad (2)$$

which characterizes a low-energy patch model with the radial cutoff Λ_k around each saddle point [Fig. 2(c)].

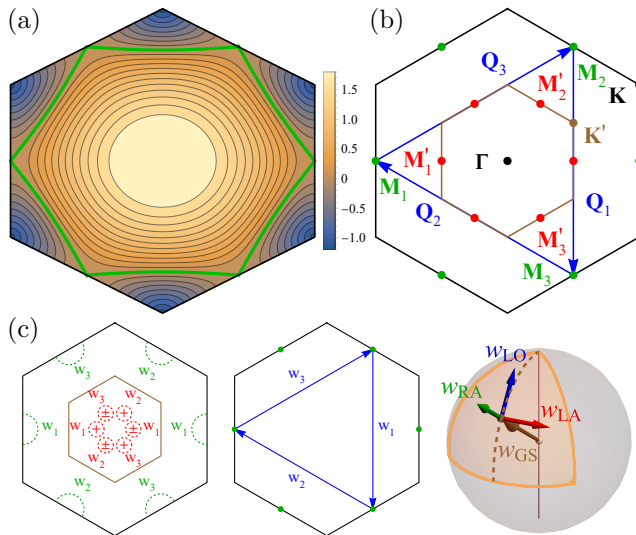


FIG. 2. Model setup. (a) The middle band of the kagome lattice with the (green) VH Fermi surface in the (black) BZ. In addition to the nearest-neighbor hopping $t_1 = 1$, we introduce an intrasublattice hopping $t_2 = 0.05$ between next-nearest-neighbor unit cells to induce the nonperfect nesting. (b) High-symmetry points and nesting momenta in the (black) original and (brown) reduced BZs. (c) In the patch models (left) and at the nesting momenta (middle), the symmetry channels can be mapped onto a Bloch sphere (right).

V_{CDW} defines the projected interaction in the CDW channel. The phase diagram (Fig. 1) [35] is consistent with the intuition from the Ginzburg-Landau theory [33–35]. Near the VHS, the CDW expands a strong $3Q+$ phase with high critical temperature T_{CDW} . These $3Q+$ orders develop the simultaneous ordering $|\Delta_1| = |\Delta_2| = |\Delta_3|$ under $\Delta_1\Delta_2\Delta_3 > 0$, which maximizes the gap structures by opening the gaps at the Fermi level [34, 45]. In practical systems, the Fermi level usually lies away from the VHS. The nonzero doping $\mu \neq 0$ can draw the reconstructed Fermi surface and alter the energetic favor. While the $3Q+$ orders remain stable at negative doping $\mu < 0$, the $3Q-$ orders with $\Delta_1\Delta_2\Delta_3 < 0$ can emerge at positive doping $\mu > 0$. Near the phase transition, the CDW is pinned to the $1Q$ orders at single momenta. The nonzero doping suppresses the CDW phase and reduces the critical temperature T_{CDW} gradually. This is attributed to the reduction of the density of states and Fermi surface nesting. When the CDW vanishes at the critical dopings, the ground state returns to the $0Q$ normal metal (NM). Note that different phases are separated by the first-order transitions, where the ground state switches abruptly between different orders. While the phase diagram has been presented previously [35], we further show that it contains several properties essential to the multidome superconductivity.

Remarkably, the CDW phase can be suppressed by different variations in the kagome metals AV_3Sb_5 . In addition to the nonzero doping [23], the suppression was also observed under pressure [6, 8, 24, 27] and uniaxial strain [29]. These effects may be related to the Fermi level shifting [6] or the interaction reduction under structural variation [18]. In the low-energy theory, the variations can be summarized by the tunings of doping, Fermi surface nesting, and interaction strength. We model these effects by a single parameter, which defines the shifting away from the perfectly nested VHS at a fixed dimensionless interaction. The shifting further determines the reduction of the critical temperature T_{CDW} . Our analysis adopts the doping μ as the tunable parameter. This setup supports a tunable framework where the properties of the suppressed CDW phase can be examined.

We are interested in the reconstructed Fermi surface under nonzero doping. To obtain the reconstructed band structure, we adopt the ground state of the effective Hamiltonian (2) to a full four-band mean-field Hamiltonian in the reduced BZ [34]. The choice of an $(s+d)$ -wave form factor diminishes the CDW away from the Fermi level. Despite the mismatch in the model details, the computation captures the essential features of the reconstructed band structure. We monitor the evolution of the density of states $D(\mu)$ [Fig. 3(a)] and map out the reconstructed Fermi surface [Fig. 3(b)] at zero temperature $T = 0$. In the $3Q+$ phase, the small \mathbf{M}'_{α} pockets appear under the gaps at the Fermi level. The increasing doping enlarges the \mathbf{M}'_{α} pockets and raises the

density of states. Importantly, the enlarged \mathbf{M}'_α pockets lose the energetic favor to the \mathbf{K}'_α pockets at sufficiently large positive doping $\mu > 0$. This corresponds to a transition to the $3Q-$ phase. A Lifshitz transition is naturally expected between the two phases, which hosts a reconstructed VHS. Although this transition is covered by an intermediate $1Q$ phase in our model, the proximity to the reconstructed VHS still enhances the density of states significantly. On the other hand, the reconstructed Fermi surface recovers its noninteracting form at the critical dopings. With the closeness to the VHS, the density of states is again elevated. Note that the reconstructed Fermi surface changes abruptly at the first-order transitions. Correspondingly, the density of states experiences sharp jumps at the regime boundaries.

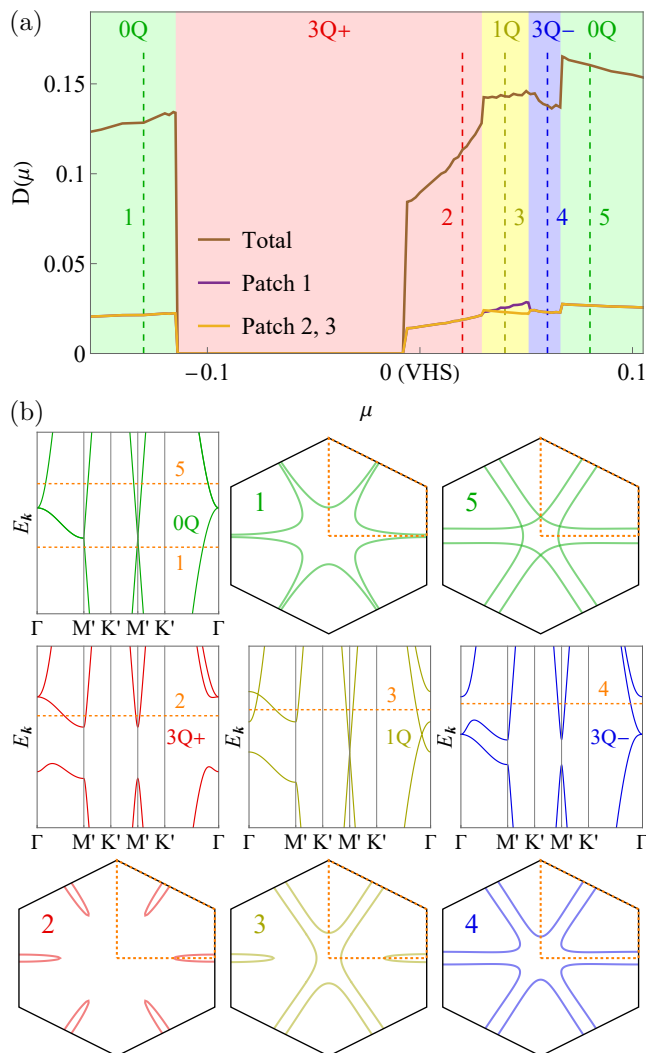


FIG. 3. Reconstructed Fermi surface under the parent CDW at $T = 0$. We compute the density of states (a) and obtain the reconstructed band structure and Fermi surface (b). The density of states at each patch D_α is estimated by the total in each $\Gamma\text{-}\mathbf{K}'\text{-}\mathbf{K}'$ $1/6$ subzone.

Due to the presence of multiple transitions, the reconstructed metallic phase is divided into multiple regimes. Whether each regime appears is system dependent. Interestingly, the transitions between different CDW phases were observed under pressure [6, 8, 24, 27]. Furthermore, the reconstructed VHS was probed close to the Fermi level for $A = \text{Rb}$ [21]. The multiregime nature of the reconstructed metal is essential to the low-energy phenomena.

Multidome superconductivity.—As a central spirit of our work, we propose that the superconductivity develops as a weak-coupling instability on the reconstructed Fermi surface. This establishes a ‘parent-child relationship’ between the CDW and the superconductivity, where the large separation of energy scales is naturally explained. Moreover, the multiregime reconstructed metal naturally hosts the intriguing multidome superconductivity. Deep in the CDW phase, the small density of states under the $3Q+$ orders supports the superconductivity at low critical temperature T_{SC} . As the doping increases, the increasing density of states enhances the superconductivity and raises its critical temperature T_{SC} . This is opposite to the suppression of the parent CDW phase, consistent with the experimental observations under pressure [6, 8, 24, 27], doping [23], and uniaxial strain [29]. Importantly, the reconstructed VHS can support significant enhancement and create a peak in the critical temperature T_{SC} [46, 57]. Although it is inaccessible in our model, the enhancement still manifests adequately across the $1Q$ regime. The elevated critical temperature T_{SC} depicts a superconducting dome in the parent CDW phase. When the CDW is driven across a critical doping, the superconductivity experiences another enhancement from the closeness to the VHS. This marks another superconducting dome which extends beyond the parent CDW phase. Thus our model predicts a ‘multidome’ child superconductivity from the parent CDW (Fig. 1). The double-dome structure under positive doping $\mu > 0$ is close to the observations under pressure [6, 24, 27]. Interestingly, the observed peaks are reminiscent of those from the (reconstructed) VHS. On the other hand, the double-dome structure under negative doping $\mu < 0$ was also observed [23], where the domes are separated by a sharp transition at the critical doping.

Patch model and symmetry analysis.—To further understand the superconductivity, we adopt a low-energy patch model in the reconstructed metal. The patch model takes a six-patch form, where the small patches \mathbf{p}_α capture the relevant portions of the reconstructed Fermi surface in the $\Gamma\text{-}\mathbf{K}'\text{-}\mathbf{K}'$ $1/6$ subzones [Fig. 2(c)]. The low-energy theory manifests the six-component fermion $(\psi_+^T, \psi_-^T)^T$ with $\psi_\pm = (\psi_{\pm 1}, \psi_{\pm 2}, \psi_{\pm 3})^T$. Correspondingly, the density of states reads $(D^T, D^T)^T$ with $D = (D_1, D_2, D_3)^T$. The patch model offers a natural basis for the symmetry analysis. There exist six orthonormal representations $(w_+^T, w_-^T)^T$, which correspond to the

form factors $w_{\mathbf{k}}$ in six symmetry channels. Three of the channels are even and three are odd under the inversion $w_+ = \pm w_- = w = w_{w_1 w_2 w_3}$, where $w_{w_1 w_2 w_3}$ denotes the normalized form of (w_1, w_2, w_3) . The symmetry channels are clearly illustrated by a mapping onto the Bloch sphere [Fig. 2(c)]. At the ground state (GS) w_{GS} , the characteristic orthonormal basis defines the channels as radial (RA) w_{RA} , longitudinal (LO) w_{LO} , and latitudinal (LA) w_{LA} . Under the C_3 symmetry, the ground state $w_{\text{GS}} = w_{111}$ hosts $w_{\text{RA}} = w_{111}$ along with the degenerate $w_{\text{LO}} = w_{2-1-1}$ and $w_{\text{LA}} = w_{01-1}$.

Note that the ground state may break the C_3 symmetry, such as in the $1Q$ phase. Assume the C_3 symmetry breaking at the momentum \mathbf{Q}_1 , which leads to a twofold symmetry along the x direction. The reconstructed metal holds the (possibly weak) x and y reflection symmetries. In the patch model, the twofold symmetry manifests in the anisotropic patch momenta $\mathbf{p}_1 \neq \mathbf{p}_2 = \mathbf{p}_3$ and density of states $D_1 \neq D_2 = D_3$. The ground state w_{GS} shifts away from w_{111} along the longitude on the Bloch sphere [Fig. 2(c)]. While the radial and longitudinal channels deform together in the reflection-even branch, the reflection-odd latitudinal channel remains invariant.

Pairing formalism.—We now study the superconductivity in the low-energy theory. Consider the projection of general interaction on the Cooper channels [66]

$$H_{\text{CP}} = (P_{\text{CP}}^\nu)^\dagger V_{s/t} P_{\text{CP}}^\nu. \quad (3)$$

The spin-singlet and spin-triplet Cooper pairings (CPs) are $(P_{\text{CP}}^\nu)^\dagger = \psi_{\pm\alpha}^\dagger (\sigma^\nu / \sqrt{2}) [(i\sigma^2)(\psi_{-\alpha}^\dagger)^T]$ with the spin Pauli matrices $\sigma^0 = 1$ and $\sigma^{1,2,3}$, respectively. Under the Fermi statistics, these pairings are coupled by the symmetric or antisymmetric interactions $V_{s/t} = (V_{s/t, \alpha\beta})$ with $V_{s/t, \alpha\beta} = (V_{\mathbf{p}_\alpha - \mathbf{p}_\beta} \pm V_{\mathbf{p}_\alpha + \mathbf{p}_\beta})/2$. The interaction takes a general matrix form under the twofold symmetry

$$V = \begin{pmatrix} V_1 & V_3 & V_3 \\ V_3^* & V_2 & V_4 \\ V_3^* & V_4 & V_2 \end{pmatrix}. \quad (4)$$

Here, $V_{1,2,4} \in \mathbb{R}$ and $V_3 \in \mathbb{C}$ are assumed, which matches all candidates in our analysis. Note that $V_1 = V_2$ and $V_3 = V_4$ under the C_3 symmetry.

A diagonalization determines the symmetry channels of the pairing states. In each symmetry channel

$$H_{\text{SC}} = V_{\text{SC}} (P_{\text{SC}}^\nu)^\dagger P_{\text{SC}}^\nu, \quad (5)$$

the pairing $(P_{\text{SC}}^\nu)^\dagger = \psi_{\pm}^\dagger (\sigma^\nu / \sqrt{2}) \hat{w}_{\text{SC}} [(i\sigma^2)(\psi_{\mp}^\dagger)^T]$ adopts an eigenstate $w_{\text{SC}} = \hat{w}_{\text{SC}} / |\hat{w}_{\text{SC}}|$ as the representation $\hat{w}_{\text{SC}} = \text{diag}(w_{\text{SC}})$. The projected interaction V_{SC} is given by the corresponding eigenvalue. We identify the pairing

states in six symmetry channels

Radial or longitudinal

$$V_{\text{SC}} = \frac{1}{2}(V_1 + V_\pm), \quad \tilde{w}_{\text{SC}} = \begin{pmatrix} V_1 - V_\mp \\ 2V_3^* \\ 2V_3^* \end{pmatrix}, \quad (6)$$

Latitudinal

$$V_{\text{SC}} = V_2 - V_4, \quad \tilde{w}_{\text{SC}} = \begin{pmatrix} 0 \\ 1 \\ -1 \end{pmatrix}, \quad (7)$$

with $V_\pm = V_2 + V_4 \pm \{[V_1 - (V_2 + V_4)]^2 + 8|V_3|^2\}^{1/2}$. Under the competition, the superconductivity develops from the leading pairing state with the strongest dimensionless interaction $\lambda_{\text{SC}} = V_{\text{SC}}(w_{\text{SC}}^\dagger D w_{\text{SC}}) < 0$ [67]. The critical temperature is estimated as

$$T_{\text{SC}} = \Lambda_{\text{SC}} e^{-1/|\lambda_{\text{SC}}|}, \quad (8)$$

where Λ_{SC} is an energy cutoff in the low-energy theory.

A natural question arises as which pairing states are leading in the multidome superconductivity. Since the competition is interaction dependent, the answer is strongly contingent on the pairing mechanism. Here, we discuss some candidates and their resulting pairing states in the multidome superconductivity.

Phonon-mediated attraction.—The phonon-mediated attraction always serves as a feasible candidate. Assume the weak short-range attraction with $V_{1,2,3,4} \approx V_0 < 0$. Under the C_3 symmetry, the isotropic channel w_{111} is leading. This leading channel becomes anisotropic when the twofold symmetry is manifest. Since the attraction is weakly momentum dependent, the anisotropy is weak. This contradicts with the strong anisotropy in the experimental observations [52, 53]. Therefore the phonon-mediated attraction may be an unlikely pairing mechanism.

CDW or RPOM fluctuation.—The onset from the parent CDW suggests an intriguing pairing mechanism for the superconductivity. When the parent CDW manifests a certain fluctuation, the Cooper pairs can form through its mediation at low energy. This scenario naturally matches the large separation of energy scales between the superconductivity and the CDW. The parent CDW manifests itself in the reconstruction of the band structure. At low energy, this reconstruction turns into the RPOM order on the Fermi surface. Therefore the scenario is reminiscent of the pairing from the Pomeranchuk (POM) fluctuations [68–70].

We first discuss the fluctuations of the parent CDW. Diagonalizing the free-energy Hessian matrix $(\partial_\alpha \partial_\beta f[\vec{\Delta}])_{\vec{\Delta}=\vec{\Delta}_{\text{GS}}}$ at zero temperature $T = 0$, we identify the symmetry channels of the CDW fluctuations (Fig. 4)

$$\delta f[\vec{\Delta}_{\text{GS}}] = \frac{1}{2} m^2 |\delta \vec{\Delta}|^2 \quad (9)$$

with the representation $\delta\vec{\Delta} = \delta\Delta w$ and the effective mass m^2 . Interestingly, these channels match the characteristic orthonormal basis $\{w_{\text{RA,LO,LA}}\}$ at the ground state $\vec{\Delta}_{\text{GS}} = \Delta w_{\text{GS}}$ on the Bloch sphere [Fig. 2(c)]. While the ground state exhibits the long-range CDW orders, the fluctuations exhibit the short-range correlations according to the nonzero masses.

In the parent CDW, the reconstructed metal acquires an inversion-even RPOM order $\vec{\Delta}_{\text{RPOM}} = (\Delta_{\text{RPOM}}/\sqrt{2})(w^T, w^T)^T$. The RPOM order and its fluctuations correspond approximately to the CDW ones. Due to the positive semidefiniteness, the mapping onto the Bloch sphere now occurs in the first octant [Fig. 2(c)]. The fluctuation in each symmetry channel is described by an effective charge density (CD) coupling [65, 71]

$$H_{\delta\Delta_{\text{CD}}} = \sum_{\mathbf{q}} \chi_{\mathbf{q}}^{-1} \delta\Delta_{\text{CD},-\mathbf{q}} \delta\Delta_{\text{CD},\mathbf{q}}. \quad (10)$$

The susceptibility $\chi_{\mathbf{q}} > 0$ is a result of tracing out the high-energy modes beyond the patch model. While the model involves the fluctuations at general momentum \mathbf{q} , we assume that the susceptibility peaks nondivergently $\chi_{\mathbf{q}=\mathbf{0}} \approx 2/m^2$ at zero momentum. The fluctuation couples to the CD pairing $P_{\text{CD},\mathbf{q}} = \sum_{\mathbf{k}} \psi_{\mathbf{k}+\mathbf{q}}^\dagger (\sigma^0/\sqrt{2}) w_{\mathbf{k},-\mathbf{q}} \psi_{\mathbf{k}}$ as

$$H_{\psi\delta\Delta_{\text{CD}}} = g \sum_{\mathbf{q}} P_{\text{CD},\mathbf{q}} \delta\Delta_{\text{CD},-\mathbf{q}}, \quad (11)$$

where $w_{\mathbf{k},\mathbf{q}} \sim \delta\langle \psi_{\mathbf{k}+\mathbf{q}}^\dagger \psi_{\mathbf{k}} \rangle$ is the form factor and g is an effective coupling. Integrating out the fluctuation, we arrive at an effective attraction

$$H_{\text{CD}} = -g^2 \sum_{\mathbf{q}} \chi_{\mathbf{q}} P_{\text{CD},\mathbf{q}} P_{\text{CD},-\mathbf{q}}. \quad (12)$$

It is worth discussing the structure of the form factor $w_{\mathbf{k},\mathbf{q}}$. The diagonal components $w_{\mathbf{p}_\alpha,\mathbf{q}=\mathbf{0}} = \hat{w}_{\alpha\alpha} = w_\alpha$ correspond to the intrapatch RPOM representations.

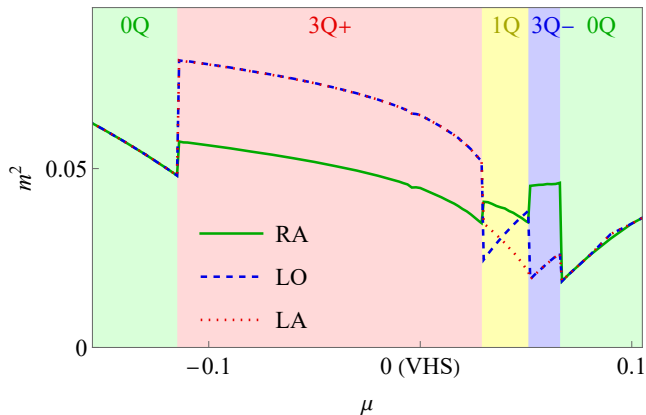


FIG. 4. The masses of the CDW fluctuations at $T = 0$.

Meanwhile, the off-diagonal components $w_{\mathbf{p}_\alpha,\mathbf{q}=\mathbf{p}_\beta-\mathbf{p}_\alpha} = \hat{w}_{\beta\alpha} = \hat{w}_{\alpha\beta}^*$ with $\alpha \neq \beta$ are interpatch. Although the incommensurate momenta $\mathbf{p}_\beta - \mathbf{p}_\alpha$ suggest the generally complex nature of the off-diagonal components $\hat{w}_{\beta\alpha}$, the symmetries can fix some of the complex phases. While the inversion evenness implies $\hat{w}_{\beta\alpha} = \hat{w}_{-\beta,-\alpha}$, the reflection evenness or oddness forces $\hat{w}_{\alpha\beta} = \pm \hat{w}_{\tilde{\alpha}\tilde{\beta}}$ for the reflection pairs $(\alpha, \tilde{\alpha})$ and $(\beta, \tilde{\beta})$. In the C_3 symmetric channel $w = w_{111}$, the off-diagonal components are $(\hat{w}_{2\pm 3}, \hat{w}_{3\pm 1}, \hat{w}_{1\pm 2}) = w_{111}$. On the other hand, the anisotropic channels may allow complex components due to the loss of certain reflection symmetries. Enforcing the reality, we find the components $(\hat{w}_{2\pm 3}, \hat{w}_{3\pm 1}, \hat{w}_{1\pm 2}) = w_{abb}$ with $a, b \in \mathbb{R}$ and w_{01-1} in the reflection-even and reflection-odd channels, respectively.

We now project the effective attraction on the Cooper channels

$$H_{\text{CP}} = -g^2 \sum_{\alpha\beta} \chi_{\alpha\beta} \hat{w}_{\beta\alpha} \hat{w}_{-\beta-\alpha} \psi_\alpha^\dagger \psi_{-\alpha}^\dagger \psi_{-\beta} \psi_\beta. \quad (13)$$

Here $\chi_{\alpha\beta} = \chi_{\mathbf{q}=\mathbf{p}_\alpha-\mathbf{p}_\beta}$, and the four-fermion spin indices $(\sigma, \sigma', \sigma', \sigma)$ are suppressed. The symmetric or antisymmetric interactions read

$$V_{\alpha\beta} = -g^2 (\chi_{\alpha\beta} \hat{w}_{\beta\alpha}^2 \pm \chi_{\alpha-\beta} \hat{w}_{-\beta\alpha}^2). \quad (14)$$

Since the symmetric interactions are generally stronger, the spin-singlet pairings are energetically favorable. The diagonal RPOM components determine the symmetry channels of the pairing states. Meanwhile, the off-diagonal components perturb these channels and break the possible degeneracy. The leading pairing state is chosen by the strongest dimensionless interaction

$$|\lambda_{\text{SC}}| = C_{\text{SC}} m^{-2} V_{w,\text{SC}} (w_{\text{SC}}^\dagger D w_{\text{SC}}), \quad (15)$$

which does not necessarily originate from the leading fluctuation. Here, C_{SC} is an effective parameter, and $V_{w,\text{SC}}$ is an eigenvalue of the dominant interaction representation $\text{diag}(w_1^2, w_2^2, w_3^2)$. Note that the CDW fluctuations can also trigger the superconductivity in the 0Q normal metal. With the unfolded patch model at \mathbf{M}_α , the symmetry channels are dominated by the off-diagonal CDW components.

Remarkably, the pairing states with the strongly anisotropic twofold structures $w_{\text{SC}} = w_{1\delta\delta,\delta 11}$ can be leading in the multidome superconductivity (Table I). Here, $0 < \delta \ll 1$ (may be complex under the twofold symmetry) represents the infinitesimal components from the off-diagonal perturbations. Since the CDW breaks the C_3 symmetry in the kagome metals AV_3Sb_5 , the twofold structures are pinned along a single direction in the parent CDW phase. Interestingly, the twofold structures were observed in the magnetoresistance measurement [52, 53]. Furthermore, the sign preservation matches the scanning tunneling microscopy and spectroscopy [54]. While a thermal conductivity measurement suggested a nodal gap [49], the measurements of

GS	w_{GS}	Fluctuation \rightarrow pairing state w_{SC}
In parent CDW phase		
$3Q+$	w_{111}	$w_{LO} \rightarrow w_{1\delta\delta} > w_{LA} \rightarrow \{w_{\delta 11} \gtrsim w_{01-1}\}$
$1Q$	w_{100}	$w_{RA} \rightarrow w_{1\delta\delta} > w_{LO/LA} \rightarrow \{w_{\delta 11} \gtrsim w_{01-1}\}$
$3Q-$	$w_{\mp 111}$	$w_{LO} \rightarrow w_{1\delta\delta} > w_{LA} \rightarrow \{w_{\delta 11} \gtrsim w_{01-1}\}$
Beyond parent CDW phase		
$0Q$	w_{000}	$w_{RA/LO/LA} = w_{100,010,001} \rightarrow w_{011,101,110}$

TABLE I. Leading pairing states from the CDW or RPOM fluctuations in the multidome superconductivity. Here, $w_1 > w_2$ means that w_1 and w_2 are the leading and secondary channels, respectively, and $\{w_1 \gtrsim w_2\}$ represents the degeneracy with perturbative breakdown. The \mp sign in the $3Q-$ phase corresponds to the CDW or RPOM description.

magnetic penetration depth and specific heat caused an opposite conclusion to be drawn [50]. This contradiction may originate from the infinitesimal component δ . Beyond the parent CDW phase, the degenerate pairing states $w_{011,101,110}$ may form the nodeless ground states with possible time-reversal symmetry breaking.

Finally, we note some features of the critical temperature T_{SC} from the CDW or RPOM fluctuations. The competition between different channels can broaden the transition temperature window between T_{SC}^{onset} and T_{SC}^{zero} [6, 24, 27], where the resistivity drops and vanishes, respectively. Meanwhile, the enhanced fluctuations at the first-order transitions can strengthen the peaks of the critical temperature T_{SC} at the regime boundaries.

Discussion.—We show that the parent CDW naturally hosts the multidome child superconductivity in the kagome metals AV_3Sb_5 . The ‘parent-child relationship’ realizes the large separation of energy scales between the superconductivity and the CDW. Meanwhile, the multidome superconductivity originates from the multi-regime reconstructed metal with distinct (reconstructed) VHSs. The pairing states with strong twofold anisotropy can develop from the CDW or RPOM fluctuations. Our work sheds light on an unconventional pairing mechanism with strong evidence in the kagome metals AV_3Sb_5 .

Our analysis is exemplified with a real CDW on a two-dimensional single-orbital kagome lattice. The inclusion of three-dimensional multiband orders may yield a more accurate description of the kagome metals AV_3Sb_5 , such as the general involvement of twofold symmetry [39] and the access to the reconstructed VHS. A combination with an imaginary CDW [34] can further incorporate the time-reversal symmetry breaking. Meanwhile, the possible band topology [2, 3, 7, 34, 40, 47] can make the superconductivity geometrically enhanced [72–76] or topological [77]. Spin-orbit coupling may also lead to additional features. Note that the multidome structure follows solely from the evolution of the density of states, which will be shared by any weak-coupling pairing mechanism on the reconstructed Fermi surface. If the ferromagnetic fluctuation or the Kohn-Luttinger renormalization [62, 66] is

strong, the spin-triplet pairing states may develop. On the other hand, the first-order transitions may hinder the quantum critical behavior at the regime boundaries [78, 79]. The related discussion is beyond our mean-field framework and is an interesting topic for future work. Finally, since the VH Fermi surface is universal on the hexagonal lattices, our analysis is also applicable to the other hexagonal-lattice systems.

Note added. Recently, we learned about an independent study of kagome superconductors from CDW fluctuations [80]. This work considered the unfolded unreconstructed theory, which is eligible outside the CDW. We adopt the folded reconstructed theory in the parent CDW phase. This captures more precisely the situation in the kagome metals AV_3Sb_5 and explains the double-dome superconductivity. Furthermore, our work conducts a systematic symmetry analysis of the multi- Q CDW orders and their fluctuations. This determines the leading pairing states with strong experimental relevance in a complete framework.

This research was sponsored by the Army Research Office and was accomplished under Grant No. W911NF-17-1-0482. The views and conclusions contained in this document are those of the authors and should not be interpreted as representing the official policies, either expressed or implied, of the Army Research Office or the U.S. Government. The U.S. Government is authorized to reproduce and distribute reprints for Government purposes notwithstanding any copyright notation herein. RN also acknowledges the support of the Alfred P. Sloan foundation through a Sloan Research Fellowship.

-
- [1] B. R. Ortiz, L. C. Gomes, J. R. Morey, M. Winiarski, M. Bordelon, J. S. Mangum, I. W. H. Oswald, J. A. Rodriguez-Rivera, J. R. Neilson, S. D. Wilson, E. Ertekin, T. M. McQueen, and E. S. Toberer, New kagome prototype materials: discovery of KV_3Sb_5 , RbV_3Sb_5 , and CsV_3Sb_5 , *Phys. Rev. Materials* **3**, 094407 (2019).
 - [2] S.-Y. Yang, Y. Wang, B. R. Ortiz, D. Liu, J. Gayles, E. Derunova, R. Gonzalez-Hernandez, L. Šmejkal, Y. Chen, S. S. P. Parkin, S. D. Wilson, E. S. Toberer, T. McQueen, and M. N. Ali, Giant, unconventional anomalous Hall effect in the metallic frustrated magnet candidate, KV_3Sb_5 , *Sci. Adv.* **6**, eabb6003 (2020).
 - [3] B. R. Ortiz, S. M. L. Teicher, Y. Hu, J. L. Zuo, P. M. Sarte, E. C. Schueller, A. M. M. Abeykoon, M. J. Krogstad, S. Rosenkranz, R. Osborn, R. Seshadri, L. Balents, J. He, and S. D. Wilson, CsV_3Sb_5 : A Z_2 Topological Kagome Metal with a Superconducting Ground State, *Phys. Rev. Lett.* **125**, 247002 (2020).
 - [4] E. M. Kenney, B. R. Ortiz, C. Wang, S. D. Wilson, and M. J. Graf, Absence of local moments in the kagome metal KV_3Sb_5 as determined by muon spin spectroscopy, *J. Phys.: Condens. Matter* **33**, 235801 (2021).
 - [5] Y.-X. Jiang, J.-X. Yin, M. M. Denner, N. Shumiya, B. R.

- Ortiz, G. Xu, Z. Guguchia, J. He, M. S. Hossain, X. Liu, J. Ruff, L. Kautzsch, S. S. Zhang, G. Chang, I. Belopolski, Q. Zhang, T. A. Cochran, D. Multer, M. Litskevich, Z.-J. Cheng, X. P. Yang, Z. Wang, R. Thomale, T. Neupert, S. D. Wilson, and M. Zahid Hasan, Unconventional chiral charge order in kagome superconductor KV_3Sb_5 , *Nat. Mater.* **20**, 1353 (2021).
- [6] K. Y. Chen, N. N. Wang, Q. W. Yin, Y. H. Gu, K. Jiang, Z. J. Tu, C. S. Gong, Y. Uwatoko, J. P. Sun, H. C. Lei, J. P. Hu, and J.-G. Cheng, Double Superconducting Dome and Triple Enhancement of T_c in the Kagome Superconductor CsV_3Sb_5 under High Pressure, *Phys. Rev. Lett.* **126**, 247001 (2021).
- [7] F. H. Yu, T. Wu, Z. Y. Wang, B. Lei, W. Z. Zhuo, J. J. Ying, and X. H. Chen, Concurrence of anomalous hall effect and charge density wave in a superconducting topological kagome metal, *Phys. Rev. B* **104**, L041103 (2021).
- [8] F. Du, S. Luo, B. R. Ortiz, Y. Chen, W. Duan, D. Zhang, X. Lu, S. D. Wilson, Y. Song, and H. Yuan, Pressure-induced double superconducting domes and charge instability in the kagome metal KV_3Sb_5 , *Phys. Rev. B* **103**, L220504 (2021).
- [9] H. Zhao, H. Li, B. R. Ortiz, S. M. L. Teicher, T. Park, M. Ye, Z. Wang, L. Balents, S. D. Wilson, and I. Zeljkovic, Cascade of correlated electron states in a kagome superconductor CsV_3Sb_5 , *Nature* **599**, 216 (2021).
- [10] Z. Liang, X. Hou, F. Zhang, W. Ma, P. Wu, Z. Zhang, F. Yu, J.-J. Ying, K. Jiang, L. Shan, Z. Wang, and X.-H. Chen, Three-Dimensional Charge Density Wave and Surface-Dependent Vortex-Core States in a Kagome Superconductor CsV_3Sb_5 , *Phys. Rev. X* **11**, 031026 (2021).
- [11] E. Uykur, B. R. Ortiz, S. D. Wilson, M. Dressel, and A. A. Tsirlin, Optical detection of the density-wave instability in the kagome metal KV_3Sb_5 , *npj Quantum Mater.* **7**, 16 (2022).
- [12] H. Chen, H. Yang, B. Hu, Z. Zhao, J. Yuan, Y. Xing, G. Qian, Z. Huang, G. Li, Y. Ye, S. Ma, S. Ni, H. Zhang, Q. Yin, C. Gong, Z. Tu, H. Lei, H. Tan, S. Zhou, C. Shen, X. Dong, B. Yan, Z. Wang, and H.-J. Gao, Roton pair density wave in a strong-coupling kagome superconductor, *Nature* **599**, 222 (2021).
- [13] H. Li, T. T. Zhang, T. Yilmaz, Y. Y. Pai, C. E. Marvinney, A. Said, Q. W. Yin, C. S. Gong, Z. J. Tu, E. Vescovo, C. S. Nelson, R. G. Moore, S. Murakami, H. C. Lei, H. N. Lee, B. J. Lawrie, and H. Miao, Observation of Unconventional Charge Density Wave without Acoustic Phonon Anomaly in Kagome Superconductors AV_3Sb_5 ($A = Rb, Cs$), *Phys. Rev. X* **11**, 031050 (2021).
- [14] Z. Wang, S. Ma, Y. Zhang, H. Yang, Z. Zhao, Y. Ou, Y. Zhu, S. Ni, Z. Lu, H. Chen, K. Jiang, L. Yu, Y. Zhang, X. Dong, J. Hu, H.-J. Gao, and Z. Zhao, Distinctive momentum dependent charge-density-wave gap observed in CsV_3Sb_5 superconductor with topological Kagome lattice, arXiv e-prints, arXiv:2104.05556 (2021), arXiv:2104.05556 [cond-mat.supr-con].
- [15] K. Nakayama, Y. Li, T. Kato, M. Liu, Z. Wang, T. Takahashi, Y. Yao, and T. Sato, Multiple energy scales and anisotropic energy gap in the charge-density-wave phase of the kagome superconductor CsV_3Sb_5 , *Phys. Rev. B* **104**, L161112 (2021).
- [16] H. Li, H. Zhao, B. R. Ortiz, T. Park, M. Ye, L. Balents, Z. Wang, S. D. Wilson, and I. Zeljkovic, Rotation symmetry breaking in the normal state of a kagome superconductor KV_3Sb_5 , *Nat. Phys.* **18**, 265 (2021).
- [17] N. Shumiya, M. S. Hossain, J.-X. Yin, Y.-X. Jiang, B. R. Ortiz, H. Liu, Y. Shi, Q. Yin, H. Lei, S. S. Zhang, G. Chang, Q. Zhang, T. A. Cochran, D. Multer, M. Litskevich, Z.-J. Cheng, X. P. Yang, Z. Guguchia, S. D. Wilson, and M. Z. Hasan, Intrinsic nature of chiral charge order in the kagome superconductor RbV_3Sb_5 , *Phys. Rev. B* **104**, 035131 (2021).
- [18] A. A. Tsirlin, P. Fertey, B. R. Ortiz, B. Klis, V. Merkl, M. Dressel, S. D. Wilson, and E. Uykur, Role of Sb in the superconducting kagome metal CsV_3Sb_5 revealed by its anisotropic compression, *SciPost Phys.* **12**, 49 (2022).
- [19] M. Kang, S. Fang, J.-K. Kim, B. R. Ortiz, S. H. Ryu, J. Kim, J. Yoo, G. Sangiovanni, D. Di Sante, B.-G. Park, C. Jozwiak, A. Bostwick, E. Rotenberg, E. Kaxiras, S. D. Wilson, J.-H. Park, and R. Comin, Twofold van Hove singularity and origin of charge order in topological kagome superconductor CsV_3Sb_5 , *Nat. Phys.* **18**, 301 (2022).
- [20] Z. Wang, Y.-X. Jiang, J.-X. Yin, Y. Li, G.-Y. Wang, H.-L. Huang, S. Shao, J. Liu, P. Zhu, N. Shumiya, M. S. Hossain, H. Liu, Y. Shi, J. Duan, X. Li, G. Chang, P. Dai, Z. Ye, G. Xu, Y. Wang, H. Zheng, J. Jia, M. Z. Hasan, and Y. Yao, Electronic nature of chiral charge order in the kagome superconductor CsV_3Sb_5 , *Phys. Rev. B* **104**, 075148 (2021).
- [21] S. Cho, H. Ma, W. Xia, Y. Yang, Z. Liu, Z. Huang, Z. Jiang, X. Lu, J. Liu, Z. Liu, J. Li, J. Wang, Y. Liu, J. Jia, Y. Guo, J. Liu, and D. Shen, Emergence of New van Hove Singularities in the Charge Density Wave State of a Topological Kagome Metal RbV_3Sb_5 , *Phys. Rev. Lett.* **127**, 236401 (2021).
- [22] B. Q. Song, X. M. Kong, W. Xia, Q. W. Yin, C. P. Tu, C. C. Zhao, D. Z. Dai, K. Meng, Z. C. Tao, Z. J. Tu, C. S. Gong, H. C. Lei, Y. F. Guo, X. F. Yang, and S. Y. Li, Competing superconductivity and charge-density wave in Kagome metal CsV_3Sb_5 : evidence from their evolutions with sample thickness, arXiv e-prints, arXiv:2105.09248 (2021), arXiv:2105.09248 [cond-mat.supr-con].
- [23] Y. Song, T. Ying, X. Chen, X. Han, X. Wu, A. P. Schnyder, Y. Huang, J.-g. Guo, and X. Chen, Competition of Superconductivity and Charge Density Wave in Selective Oxidized CsV_3Sb_5 Thin Flakes, *Phys. Rev. Lett.* **127**, 237001 (2021).
- [24] F. H. Yu, D. H. Ma, W. Z. Zhuo, S. Q. Liu, X. K. Wen, B. Lei, J. J. Ying, and X. H. Chen, Unusual competition of superconductivity and charge-density-wave state in a compressed topological kagome metal, *Nat. Commun.* **12**, 3645 (2021).
- [25] Y. Hu, X. Wu, B. R. Ortiz, S. Ju, X. Han, J. Ma, N. C. Plumb, M. Radovic, R. Thomale, S. D. Wilson, A. P. Schnyder, and M. Shi, Rich nature of Van Hove singularities in Kagome superconductor CsV_3Sb_5 , *Nat. Commun.* **13**, 2220 (2022).
- [26] C. Mielke, D. Das, J. X. Yin, H. Liu, R. Gupta, Y. X. Jiang, M. Medarde, X. Wu, H. C. Lei, J. Chang, P. Dai, Q. Si, H. Miao, R. Thomale, T. Neupert, Y. Shi, R. Khasanov, M. Z. Hasan, H. Luetkens, and Z. Guguchia, Time-reversal symmetry-breaking charge order in a kagome superconductor, *Nature* **602**, 245 (2022).
- [27] N. N. Wang, K. Y. Chen, Q. W. Yin, Y. N. N. Ma, B. Y. Pan, X. Yang, X. Y. Ji, S. L. Wu, P. F. Shan, S. X. Xu, Z. J. Tu, C. S. Gong, G. T. Liu, G. Li, Y. Uwatoko, X. L. Dong, H. C. Lei, J. P. Sun, and J.-G. Cheng, Competi-

- tion between charge-density-wave and superconductivity in the kagome metal RbV_3Sb_5 , *Phys. Rev. Research* **3**, 043018 (2021).
- [28] H. Luo, Q. Gao, H. Liu, Y. Gu, D. Wu, C. Yi, J. Jia, S. Wu, X. Luo, Y. Xu, L. Zhao, Q. Wang, H. Mao, G. Liu, Z. Zhu, Y. Shi, K. Jiang, J. Hu, Z. Xu, and X. J. Zhou, Electronic nature of charge density wave and electron-phonon coupling in kagome superconductor KV_3Sb_5 , *Nat. Commun.* **13**, 273 (2022).
- [29] T. Qian, M. H. Christensen, C. Hu, A. Saha, B. M. Andersen, R. M. Fernandes, T. Birol, and N. Ni, Revealing the competition between charge density wave and superconductivity in CsV_3Sb_5 through uniaxial strain, *Phys. Rev. B* **104**, 144506 (2021).
- [30] L. Van Hove, The occurrence of singularities in the elastic frequency distribution of a crystal, *Phys. Rev.* **89**, 1189 (1953).
- [31] H. Tan, Y. Liu, Z. Wang, and B. Yan, Charge density waves and electronic properties of superconducting kagome metals, *Phys. Rev. Lett.* **127**, 046401 (2021).
- [32] X. Feng, K. Jiang, Z. Wang, and J. Hu, Chiral flux phase in the Kagome superconductor AV_3Sb_5 , *Sci. Bull.* **66**, 1384 (2021).
- [33] M. M. Denner, R. Thomale, and T. Neupert, Analysis of Charge Order in the Kagome Metal AV_3Sb_5 ($A = \text{K, Rb, Cs}$), *Phys. Rev. Lett.* **127**, 217601 (2021).
- [34] Y.-P. Lin and R. M. Nandkishore, Complex charge density waves at Van Hove singularity on hexagonal lattices: Haldane-model phase diagram and potential realization in the kagome metals AV_3Sb_5 ($A=\text{K, Rb, Cs}$), *Phys. Rev. B* **104**, 045122 (2021).
- [35] T. Park, M. Ye, and L. Balents, Electronic instabilities of kagome metals: Saddle points and Landau theory, *Phys. Rev. B* **104**, 035142 (2021).
- [36] C. Setty, H. Hu, L. Chen, and Q. Si, Electron correlations and T -breaking density wave order in a \mathbb{Z}_2 kagome metal, arXiv e-prints, arXiv:2105.15204 (2021), arXiv:2105.15204 [cond-mat.str-el].
- [37] X. Feng, Y. Zhang, K. Jiang, and J. Hu, Low-energy effective theory and symmetry classification of flux phases on the kagome lattice, *Phys. Rev. B* **104**, 165136 (2021).
- [38] H. Miao, H. X. Li, W. R. Meier, A. Huon, H. N. Lee, A. Said, H. C. Lei, B. R. Ortiz, S. D. Wilson, J. X. Yin, M. Z. Hasan, Z. Wang, H. Tan, and B. Yan, Geometry of the charge density wave in the kagome metal AV_3Sb_5 , *Phys. Rev. B* **104**, 195132 (2021).
- [39] M. H. Christensen, T. Birol, B. M. Andersen, and R. M. Fernandes, Theory of the charge density wave in AV_3Sb_5 kagome metals, *Phys. Rev. B* **104**, 214513 (2021).
- [40] Y.-P. Lin, Higher-order topological insulators from $3Q$ charge bond orders on hexagonal lattices: A hint to kagome metals, arXiv e-prints, arXiv:2106.09717 (2021), arXiv:2106.09717 [cond-mat.str-el].
- [41] I. Affleck and J. B. Marston, Large- n limit of the Heisenberg-Hubbard model: Implications for high- T_c superconductors, *Phys. Rev. B* **37**, 3774 (1988).
- [42] C. M. Varma, Non-Fermi-liquid states and pairing instability of a general model of copper oxide metals, *Phys. Rev. B* **55**, 14554 (1997).
- [43] C. Nayak, Density-wave states of nonzero angular momentum, *Phys. Rev. B* **62**, 4880 (2000).
- [44] S. Chakravarty, R. B. Laughlin, D. K. Morr, and C. Nayak, Hidden order in the cuprates, *Phys. Rev. B* **63**, 094503 (2001).
- [45] J. W. F. Venderbos, Symmetry analysis of translational symmetry broken density waves: Application to hexagonal lattices in two dimensions, *Phys. Rev. B* **93**, 115107 (2016).
- [46] Y.-P. Lin and R. M. Nandkishore, Chiral twist on the high- T_c phase diagram in moiré heterostructures, *Phys. Rev. B* **100**, 085136 (2019).
- [47] B. R. Ortiz, P. M. Sarte, E. M. Kenney, M. J. Graf, S. M. L. Teicher, R. Seshadri, and S. D. Wilson, Superconductivity in the \mathbb{Z}_2 kagome metal KV_3Sb_5 , *Phys. Rev. Materials* **5**, 034801 (2021).
- [48] Y. Wang, S. Yang, P. K. Sivakumar, B. R. Ortiz, S. M. L. Teicher, H. Wu, A. K. Srivastava, C. Garg, D. Liu, S. S. P. Parkin, E. S. Toberer, T. McQueen, S. D. Wilson, and M. N. Ali, Proximity-induced spin-triplet superconductivity and edge supercurrent in the topological Kagome metal, $\text{K}_{1-x}\text{V}_3\text{Sb}_5$, arXiv e-prints, arXiv:2012.05898 (2020), arXiv:2012.05898 [cond-mat.supr-con].
- [49] C. C. Zhao, L. S. Wang, W. Xia, Q. W. Yin, J. M. Ni, Y. Y. Huang, C. P. Tu, Z. C. Tao, Z. J. Tu, C. S. Gong, H. C. Lei, Y. F. Guo, X. F. Yang, and S. Y. Li, Nodal superconductivity and superconducting domes in the topological Kagome metal CsV_3Sb_5 , arXiv e-prints, arXiv:2102.08356 (2021), arXiv:2102.08356 [cond-mat.supr-con].
- [50] W. Duan, Z. Nie, S. Luo, F. Yu, B. R. Ortiz, L. Yin, H. Su, F. Du, A. Wang, Y. Chen, X. Lu, J. Ying, S. D. Wilson, X. Chen, Y. Song, and H. Yuan, Nodeless superconductivity in the kagome metal CsV_3Sb_5 , *Sci. China-Phys., Mech. Astron.* **64**, 107462 (2021).
- [51] Z. Zhang, Z. Chen, Y. Zhou, Y. Yuan, S. Wang, J. Wang, H. Yang, C. An, L. Zhang, X. Zhu, Y. Zhou, X. Chen, J. Zhou, and Z. Yang, Pressure-induced reemergence of superconductivity in the topological kagome metal CsV_3Sb_5 , *Phys. Rev. B* **103**, 224513 (2021).
- [52] S. Ni, S. Ma, Y. Zhang, J. Yuan, H. Yang, Z. Lu, N. Wang, J. Sun, Z. Zhao, D. Li, S. Liu, H. Zhang, H. Chen, K. Jin, J. Cheng, L. Yu, F. Zhou, X. Dong, J. Hu, H.-J. Gao, and Z. Zhao, Anisotropic Superconducting Properties of Kagome Metal CsV_3Sb_5 , *Chin. Phys. Lett.* **38**, 057403 (2021).
- [53] Y. Xiang, Q. Li, Y. Li, W. Xie, H. Yang, Z. Wang, Y. Yao, and H.-H. Wen, Twofold symmetry of c -axis resistivity in topological kagome superconductor CsV_3Sb_5 with in-plane rotating magnetic field, *Nat. Commun.* **12**, 6727 (2021).
- [54] H.-S. Xu, Y.-J. Yan, R. Yin, W. Xia, S. Fang, Z. Chen, Y. Li, W. Yang, Y. Guo, and D.-L. Feng, Multiband Superconductivity with Sign-Preserving Order Parameter in Kagome Superconductor CsV_3Sb_5 , *Phys. Rev. Lett.* **127**, 187004 (2021).
- [55] C. C. Zhu, X. F. Yang, W. Xia, Q. W. Yin, L. S. Wang, C. C. Zhao, D. Z. Dai, C. P. Tu, B. Q. Song, Z. C. Tao, Z. J. Tu, C. S. Gong, H. C. Lei, Y. F. Guo, and S. Y. Li, Double-dome superconductivity under pressure in the V -based kagome metals AV_3Sb_5 ($A = \text{Rb}$ and K), *Phys. Rev. B* **105**, 094507 (2022).
- [56] X. Wu, T. Schwemmer, T. Müller, A. Consiglio, G. Sangiovanni, D. Di Sante, Y. Iqbal, W. Hanke, A. P. Schnyder, M. M. Denner, M. H. Fischer, T. Neupert, and R. Thomale, Nature of Unconventional Pairing in the Kagome Superconductors AV_3Sb_5 ($A = \text{K, Rb, Cs}$), *Phys. Rev. Lett.* **127**, 177001 (2021).
- [57] R. Nandkishore, L. S. Levitov, and A. V. Chubukov,

- Chiral superconductivity from repulsive interactions in doped graphene, *Nat. Phys.* **8**, 158 (2012).
- [58] M. L. Kiesel, C. Platt, W. Hanke, D. A. Abanin, and R. Thomale, Competing many-body instabilities and unconventional superconductivity in graphene, *Phys. Rev. B* **86**, 020507 (2012).
- [59] S.-L. Yu and J.-X. Li, Chiral superconducting phase and chiral spin-density-wave phase in a hubbard model on the kagome lattice, *Phys. Rev. B* **85**, 144402 (2012).
- [60] M. L. Kiesel, C. Platt, and R. Thomale, Unconventional fermi surface instabilities in the kagome hubbard model, *Phys. Rev. Lett.* **110**, 126405 (2013).
- [61] W.-S. Wang, Z.-Z. Li, Y.-Y. Xiang, and Q.-H. Wang, Competing electronic orders on kagome lattices at van hove filling, *Phys. Rev. B* **87**, 115135 (2013).
- [62] R. Nandkishore, R. Thomale, and A. V. Chubukov, Superconductivity from weak repulsion in hexagonal lattice systems, *Phys. Rev. B* **89**, 144501 (2014).
- [63] L. Classen, A. V. Chubukov, C. Honerkamp, and M. M. Scherer, Competing orders at higher-order van hove points, *Phys. Rev. B* **102**, 125141 (2020).
- [64] Y.-P. Lin and R. M. Nandkishore, Parquet renormalization group analysis of weak-coupling instabilities with multiple high-order van hove points inside the brillouin zone, *Phys. Rev. B* **102**, 245122 (2020).
- [65] P. Coleman, *Introduction to Many-Body Physics* (Cambridge University Press, Cambridge, England, 2015).
- [66] Y.-P. Lin and R. M. Nandkishore, Kohn-luttinger superconductivity on two orbital honeycomb lattice, *Phys. Rev. B* **98**, 214521 (2018).
- [67] Y.-P. Lin, Chiral flat band superconductivity from symmetry-protected three-band crossings, *Phys. Rev. Research* **2**, 043209 (2020).
- [68] R. M. Fernandes and A. J. Millis, Nematicity as a probe of superconducting pairing in iron-based superconductors, *Phys. Rev. Lett.* **111**, 127001 (2013).
- [69] R. M. Fernandes, A. V. Chubukov, and J. Schmalian, What drives nematic order in iron-based superconductors?, *Nat. Phys.* **10**, 97 (2014).
- [70] X. Chen, S. Maiti, R. M. Fernandes, and P. J. Hirschfeld, Nematicity and superconductivity: Competition versus cooperation, *Phys. Rev. B* **102**, 184512 (2020).
- [71] A. Abanov, A. V. Chubukov, and J. Schmalian, Quantum-critical theory of the spin-fermion model and its application to cuprates: Normal state analysis, *Adv. Phys.* **52**, 119 (2003).
- [72] S. Peotta and P. Törmä, Superfluidity in topologically nontrivial flat bands, *Nat. Commun.* **6**, 8944 (2015).
- [73] L. Liang, T. I. Vanhala, S. Peotta, T. Siro, A. Harju, and P. Törmä, Band geometry, berry curvature, and superfluid weight, *Phys. Rev. B* **95**, 024515 (2017).
- [74] X. Hu, T. Hyart, D. I. Pikulin, and E. Rossi, Geometric and conventional contribution to the superfluid weight in twisted bilayer graphene, *Phys. Rev. Lett.* **123**, 237002 (2019).
- [75] F. Xie, Z. Song, B. Lian, and B. A. Bernevig, Topology-bounded superfluid weight in twisted bilayer graphene, *Phys. Rev. Lett.* **124**, 167002 (2020).
- [76] Y.-P. Lin and W.-H. Hsiao, Dual haldane sphere and quantized band geometry in chiral multifold fermions, *Phys. Rev. B* **103**, L081103 (2021).
- [77] Y. Li and F. D. M. Haldane, Topological nodal cooper pairing in doped weyl metals, *Phys. Rev. Lett.* **120**, 067003 (2018).
- [78] E. Berg, M. A. Metlitski, and S. Sachdev, Sign-problem-free quantum monte carlo of the onset of antiferromagnetism in metals, *Science* **338**, 1606 (2012).
- [79] J. P. Rodriguez, Superconductivity by hidden spin fluctuations in electron-doped iron selenide, *Phys. Rev. B* **103**, 184513 (2021).
- [80] R. Tazai, Y. Yamakawa, S. Onari, and H. Kontani, Mechanism of exotic density-wave and beyond-Migdal unconventional superconductivity in kagome metal AV_3Sb_5 ($A = K, Rb, Cs$), *Sci. Adv.* **8**, eabl4108 (2022).